Dynamic Modeling and Control of Pneumatic Artificial Muscles-Driven Multi-Fingered Robots for Circular Object Manipulation

Son Hoang [1,2], Pham Thuc Anh Nguyen [3,*], and Cong Chi Tran [4]

[1] Faculty of Electronics Engineering 1, Posts and Telecommunications Institute of Technology, Hanoi, Vietnam
[2] Automation and Robotics Laboratory (ARL Lab), Posts and Telecommunications Institute of Technology, Hanoi, Vietnam
[3] Department of Automation Engineering, School of Electrical and Electronic Engineering, Hanoi University of Science and Technology, Hanoi, Vietnam
[4] Faculty of Electromechanical and Civil Engineering, Vietnam National University of Forestry, Hanoi, Vietnam
Email: hoangson@ptit.edu.vn (S.H.); anh.nguyenphamthuc@hust.edu.vn (P.T.A.N.); trancongchi_bk@yahoo.com (C.C.T.)
*Corresponding author

***Abstract*—Recently, significant concerns have arisen regarding the application of biologically inspired robots in rehabilitation for individuals with movement disabilities. These types of robots must ensure a high level of safety, which is typically achieved through more flexible construction. Pneumatic Artificial Muscles (PAMs), driven by compressed air, exhibit performance similar to biological muscles. Consequently, PAMs are considered strong candidates for actuators in rehabilitation robots. This paper investigates a control algorithm for a multi-fingered robot actuated by PAMs for grasping and manipulating circular objects. A dynamic model of the general robot–object system was formulated using the Lagrange method, combined with the natural force–length–velocity relationship of contracting muscles. Based on this model, control algorithms were proposed to achieve stable grasping and dexterous manipulation of the object by the multi-fingered robot. The asymptotic convergence of the closed-loop system was analyzed using Lyapunov's principle and the extended LaSalle invariance theorem. Simulation results further validated the effectiveness of the proposed control algorithms.**

***Keywords*—multi-fingered robot, Pneumatic Artificial Muscle (PAM), stable grasp, dexterous manipulation, circular object**

I. Introduction

Traditional industrial robots are designed with a strong, rigid structure to perform fast, precise, and high-force operations in controlled environments like manufacturing plants [1, 2]. However, these characteristics make them potentially dangerous in biomedical applications, particularly in scenarios involving close human-robot interaction [3]. In rehabilitation settings, where robots assist individuals with movement disabilities, safety becomes a critical concern. Industrial robots lack the inherent compliance and adaptability to handle unpredictable human movements, increasing the risk of injury due to accidental collisions or excessive force [3]. These concerns have led to growing skepticism about the direct use of conventional industrial robots in medical rehabilitation, prompting the development of softer, more responsive biologically inspired robotic systems prioritizing safety and human-robot collaboration [4].

A key solution to this challenge is Pneumatic Artificial Muscles (PAMs). Specifically, electrical and hydraulic actuators with a rigid structure and behavior should be replaced by softer alternatives, such as PAMs driven by compressed air [5]. PAMs are lightweight, compliant, and capable of performing more specific tasks than comparable-sized hydraulic actuators and electrical motors [6–9]. Besides possessing all the advantages of traditional pneumatic actuators, such as low cost, fast response, and high power-to-weight and power-to-volume ratios, PAMs exhibit natural compliance, and their performance is similar to that of biological muscles. For these reasons, PAMs are considered strong candidates for actuators in rehabilitation robots [10]. To facilitate the design of controllers, the dynamics of a PAM have been constructed as a phenomenological model consisting of a contractile element, a spring element, and a damping element in parallel [11].

While initial research has explored PAM-actuated systems, significant limitations remain. For instance, a model of a robotic arm actuated by antagonistic PAM pairs highlighted the unique control properties of bio-inspired designs but did not address dynamics or control algorithms for targeted PAM-driven robots, thereby limiting its potential for real-world applications [12]. Another study presented a control

Manuscript received July 21, 2025; revised August 5, 2025; accepted September 25, 2025; published January 9, 2026.

doi: 10.18178/ijmerr.15.1.1-11

algorithm for a Two-Degree-of-Freedom (2-DOF) manipulator, but a limitation lay in its reliance on inverse kinematics, which makes the algorithm dependent on the accuracy of the system's dynamic model and parameters [13]. Subsequent controllers proposed for PAM-actuated 2-DOF manipulators were constrained to joint-level control and did not account for the Cartesian positioning of the end-effector or the interaction forces [14, 15]. Furthermore, while dual-arm robots have been developed to overcome the limits of single-armed systems [16, 17], these studies often base their control on simplified motion models that neglect the complexities of object-robot interactions and dynamic modeling and stability analysis during cooperative manipulation. Specifically, the stable grasping and coordinated control of circular objects have not been thoroughly explored.

This study proposes control algorithms for a dual-fingered robotic hand actuated by PAMs, specifically developed for grasping and manipulating circular objects. The approach enables accurate contact force control without force sensors, inspired by human blind grasping behavior. The robot–object system dynamics are formulated using the Lagrange method and Hamilton's principle, capturing the coupled interactions between the dual fingers and the manipulated object. Control schemes are designed to ensure stable grasping, with the asymptotic convergence of the closed-loop system rigorously verified through Lyapunov stability theory and the extended LaSalle invariance principle. The effectiveness of the proposed method is validated through MATLAB simulations, confirming its capability for stable and coordinated manipulation. Overall, the study establishes a mathematically grounded control framework for PAM-actuated dual-fingered robotic systems, enabling reliable manipulation of circular objects essential for tasks such as opening containers, handling tools, and assisting patients in daily activities.

The structure of this paper is outlined as follows. Section II provides a review of existing literature on PAM-driven robotic systems and dual-arm manipulation. Section III introduces the dynamics of the PAM-driven multi-fingered robot. Section IV presents the simulation results, and Section V concludes with key findings and directions for future research.

II. Literature Review

Research on biologically inspired robotics has increasingly focused on pneumatic artificial muscles due to their compliance and similarity to human muscles. Early studies modeled PAM dynamics using phenomenological approaches with contractile, spring, and damping elements. Kumamoto *et al.* [12] introduced a model of a robotic arm actuated by two antagonistic pairs of mono-articular muscles and one antagonistic pair of bi-articular muscles. Their study highlighted the unique control properties that emerged from incorporating bi-articular muscle pairs, analyzed within the framework of mechanical engineering models. The paper demonstrated the advantages of bi-articular muscles—considered essential in human motion control—and applied them to robotic manipulator control. However, the study did not address the dynamics or control algorithms for targeted PAM-driven robots, limiting its applicability to real-world scenarios. Oh and Hori [13] presented a control algorithm for a 2-DOF robotic manipulator actuated by mono-articular and bi-articular muscle-like torque inputs. They established a relationship between the endpoint force/position and the three muscle torques, with a feedforward component that incorporated inverse dynamics derived from the muscle torque models to enhance motion control. Nevertheless, a key limitation of their method was its reliance on inverse kinematics, making the algorithm highly dependent on the accuracy of the system's dynamic model and parameters. Subsequently, Kawai proposed several control approaches, including a passivity-based controller and the Robust Integral of the Sign of the Error (RISE) controller [14, 15]. However, the proposed algorithm was constrained to joint-level control. It did not account for the Cartesian positioning of the end-effector or the interaction forces between the end-effector and the manipulated object. These limitations highlight the need for further development to extend the framework toward complete spatial and force-aware manipulation.

The robots discussed above are single-armed manipulation systems, which tend to struggle with tasks requiring two-handed coordination, such as opening or closing a bottle, folding papers, or tying cables. In everyday life, most human activities rely on the coordinated use of both arms. Dual-arm robots aim to overcome these limitations by enabling more precise, coordinated manipulation, improving handling of flexible objects, and facilitating learning from human demonstrations. Wang *et al.* [16] developed a rigid-flexible dual-arm robot for safe human-robot hugging, combining a rigid frame with pneumatic muscles and variable stiffness joints. Experiments confirmed its ability to deliver safe and responsive interactions. In a different approach, Wang and Xu [17] developed a dual-arm soft robotic manipulator driven by pneumatic actuators, with each arm composed of modular soft segments. Controlled via visual servo, the system demonstrated high flexibility and adaptability in assembly tasks. Numerous other studies have also explored this direction [18–21]. A key strength of this body of work is the demonstration of hardware safety and flexibility. However, a significant weakness is that these studies often base their control on simplified motion models that neglect the complexities of object-robot interactions and dynamic modeling and stability analysis during cooperative manipulation. Specifically, the stable grasping and coordinated control of circular objects, common in real-world applications, have not been thoroughly explored. While some control strategies exist for PAM-driven systems, few offer theoretical stability guarantees in multi-arm, object-interactive contexts.

Dual-arm robots offer clear advantages over single-arm systems, yet they still fall short of replicating the dexterity of human fingers. Multi-fingered robotic hands offer a distinct advantage by enabling fine-grained

control and in-hand manipulation, which are essential for handling delicate objects and performing tasks that require nuanced motor skills [22]. However, a persistent challenge across all PAM-actuated systems is the control of interaction forces. While prior studies have extensively explored the use of PAMs in soft robotic systems, most of these works focus on performing free-space motions without interaction with external objects or environments [23, 24]. As a result, the control of interaction forces remains an open challenge. For example, a neural feedforward PID controller was developed to enhance force output performance in a 2-DOF PAM manipulator, but this force control algorithm requires force sensing, which increases system complexity and cost [25]. This reliance on sensing presents a practical barrier to widespread adoption.

The literature reveals a clear trajectory from rigid, single-arm systems towards compliant, multi-limb systems. Existing research has successfully established the mechanical feasibility and basic control of PAM-actuated robots. However, a critical gap remains between demonstrated hardware capabilities and the availability of robust, theoretically-sound control frameworks. Specifically, there is a lack of control strategies that:

(1) Explicitly model the dynamics of the robot-object system during cooperative tasks like grasping circular objects;
(2) Provide rigorous theoretical guarantees of stability using tools like Lyapunov theory;
(3) Achieve reliable force control without depending on force sensors.

The present study is situated within this gap. It builds upon the foundational work in PAM modeling and the advancements in multi-limb system design but addresses their key limitations by developing a dynamic model for a dual-fingered hand and proposing a sensorless control law with Lyapunov-based stability proofs, directly addressing the need for mathematically grounded and practical control frameworks.

III. Dynamics of PAM-Driven Multi-Fingered Robot

A. Proposed PAM-Driven Multi-Fingered Robot in Manipulating a Circular Object

The objective robot consists of two single-fingers, each finger consists of three links L_{ij} and three joints J_{ij} (for i = 1–3, j = 1–3) as shown in Fig. 1.

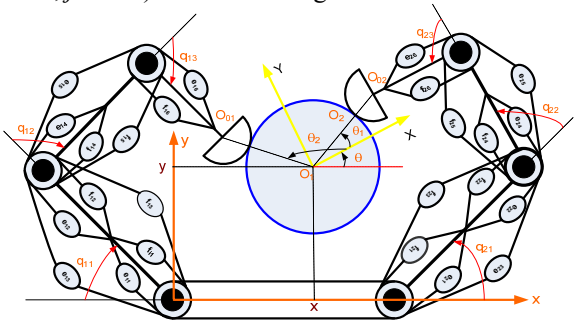

Fig. 1. Dual-fingered robot actuated by antagonistic pairs of mono- and bi-articular muscles.

For each arm i = 1, 2, two pairs of antagonistic mono-articular muscles (f_{i1}, e_{i1} and f_{i2}, e_{i2}) are mounted on joints J_{i1} and J_{i2}, respectively. Additionally, one pair of antagonistic bi-articular muscles (f_{i3}, e_{i3}) spans both joints J_{i1} and J_{i2}. At joint J_{i2}, another pair of mono-articular muscles (f_{i4}, e_{i4}) is installed. A pair of bi-articular muscles (f_{i5}, e_{i5}) connects joints J_{i2} and J_{i3}, while the final pair (f_{i6}, e_{i6}) is mounted on joint J_{i3}.

The coordinate frame {oxy} is mounted at the rotation axis of the first joint on the left arm, serving as the base reference of the system. The object frame {OXY} is located at the center of mass of the object, denoted as $O_{c.m}$. The angle between the two coordinate frames is represented by θ.

Let $q_i = (q_{i1}, q_{i2}, q_{i3})^T$ be the joint vector of the ith arm. Let define the end point of last link of ith arm X_{0i} and their position (x_{0i}, y_{0i}) in the base frame. At each contact point between the end-effector i and the object, we set coordinate frames {$O_iX_iY_i$} where the X_i directs to the origin O of the object frame. The rotational angle between the contact frame {$O_iX_iY_i$} and the object frame are defined as θ_i (for i = 1–2). Based on these definitions, the geometric constraints can be expressed as Eqs. (1) and (2):

$$Q_i = (x - x_{0i})\cos(\theta + \theta_i) + (y - y_{0i})\sin(\theta + \theta_i) + (R + r) = 0 \quad (1)$$

$$Y_i' = -(x - x_{0i})\sin(\theta + \theta_i) + (y - y_{0i})\cos(\theta + \theta_i) = 0 \quad (2)$$

where $e_i = (1, 1, 1)^T$ and c_{0i} (for i = 1–2) are constants depending on the initial state of the dual arm-object system. These constrains are associated with two elements of the interactional forces. The constraints Q_i with normal forces f_i directing from the contact point X_i to the origin O of the object are for keeping contact with the object. The constraints R_i with the tangential forces λ_i are for preventing slipping from the object surfaces. We assume that the contacts between the object and two end-effectors are rolling. The rolling contact condition should satisfy the relation given in Eq. (3):

$$\begin{aligned} R_1 &= Y_1' - c_{01} - r(\theta + \theta_1 - q_1^T e_1 - \pi) + R\theta = 0 \\ R_2 &= Y_2' - c_{02} - r(\theta + \theta_2 + q_2^T e_2) - R\theta = 0 \end{aligned} \quad (3)$$

There are two components in the dynamics of the dual-arm robot:

(1) The dynamics of the mechanical system consisting of the left arm, the right arm, the object;
(2) The dynamics of actuators driven for the dual-arm.

B. The Dynamics of the Robot-Object System without Considering PAMs

The mechanical system, excluding all PAMs, is illustrated in Fig. 2. The dynamic equations of the system are developed using the Lagrange method combined with Hamilton's principle. The Lagrangian function is defined as Eq. (4).

$$L = K - P + Q + R \tag{4}$$

where K denotes the kinetic energy, defined in Eq. (5):

$$K = \frac{1}{2}\sum_{i=1}^{2} \dot{q}_i^T H(q_i)\dot{q}_i + \left(M\dot{x}^2 + M\dot{y}^2 + I\dot{\theta}^2\right) \tag{5}$$

The potential energy P is considered zero based on the assumption that the system operates entirely within a horizontal plane. The scalar functions Q and R, derived from the constraint conditions Q_i and R_i, are formulated using Lagrange multipliers λ_i and f_i, as given in Eqs. (6) and (7):

$$Q = \sum_{i=1}^{2} f_i Q_i\,(q_i, x, y, \theta) \tag{6}$$

$$R = \sum_{i=1}^{2} \lambda_i R_i\,(q_i, x, y, \theta) \tag{7}$$

The partial derivatives of Q and R with respect to q_i are given in Eqs. (8) and (9):

$$\frac{\partial Q_i}{\partial q_i} = -J_{0i}^T \begin{bmatrix} cos(\theta + \theta_i) \\ sin(\theta + \theta_i) \end{bmatrix} \tag{8}$$

$$\frac{\partial R_i}{\partial q_i} = J_{0i}^T \begin{bmatrix} sin(\theta + \theta_i) \\ -cos(\theta + \theta_i) \end{bmatrix} - r_i \tag{9}$$

Next, by applying Hamilton's principle to the Lagrangian function L, the dynamic equations of the dual-arm system and the manipulated object are obtained. These are presented as Eq. (10) for the dual arms and Eq. (11) for the object.

$$T_i = H_i(q_i)\ddot{q}_i + \left(\frac{1}{2}\dot{H}(q_i) + S(q_i, \dot{q}_i)\right)\dot{q}_i + J_{0i}^T \begin{bmatrix} cos(\theta + \theta_i) \\ sin(\theta + \theta_i) \end{bmatrix} f_i + \left(re_i - J_{0i}^T \begin{bmatrix} sin(\theta + \theta_i) \\ -cos(\theta + \theta_i) \end{bmatrix}\right)\lambda_i \tag{10}$$

$$\begin{aligned} M\ddot{x} - f_1\,cos(\theta + \theta_1) - f_2\,cos(\theta + \theta_2) \\ +\lambda_1\,sin(\theta + \theta_1) + \lambda_2\,sin(\theta + \theta_2) = 0 \\ M\ddot{y} - f_1\,sin(\theta + \theta_1) - f_2\,sin(\theta + \theta_2) \\ -\lambda_1\,cos(\theta + \theta_1) - \lambda_2\,cos(\theta + \theta_2) = 0 \\ I\ddot{\theta} + (\lambda_1 - \lambda_2)R = 0 \end{aligned} \tag{11}$$

where J_{0i} (for i = 1, 2) are Jacobian matrices defined as:

$$J_{0i} = \begin{bmatrix} \frac{\partial x_{0i}}{\partial q_i} & \frac{\partial y_{0i}}{\partial q_i} \end{bmatrix}^T$$

where $H_i(q) \in \mathbb{R}^{n\times n}$ are inertia matrices, $S_i(q, \dot{q}) \in \mathbb{R}^{n\times n}$ are skew-symmetric matrices.

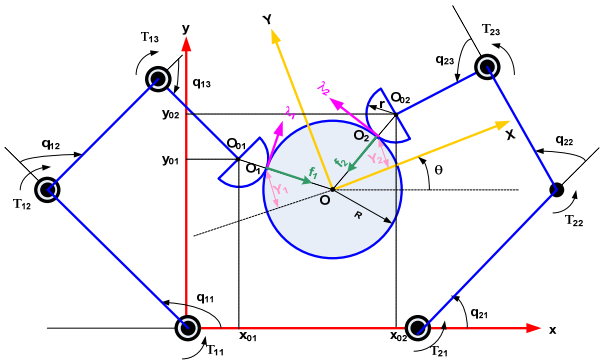

Fig. 2. Multi-fingered robot grasp a rigid circular object.

C. Formulating of the Dynamics of the Actuators

The viscous-elastic-contractile model of PAM in Fig. 3 was demonstrated by Reynolds [7]:

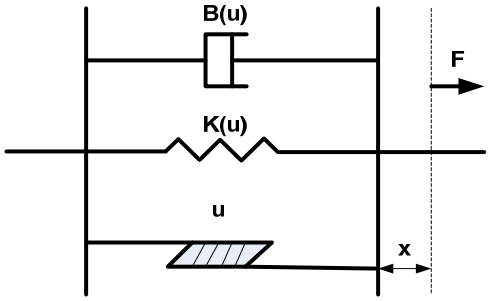

Fig. 3. Schematic of the viscoelastic contractile muscle model.

The generated output force F, governed by the contractile force u, is presented in Eq. (12).

$$F = u - kux - bu\dot{x} \tag{12}$$

where x denotes the contraction length of the muscle, and $\dot{x}$ represents the shortening velocity. The parameters k and b correspond to the elastic and viscous coefficients, respectively. Among these elements, the contractile force u is the only actively controlled component, while the others function passively. Therefore, u is regarded as the active activation level of the muscle. To generate bidirectional force, muscles must be arranged in an antagonistic configuration, typically in pairs denoted as e_{ij} and f_{ij}.

Refer to the Fig. 1, the phenomenological model of the ith arm can be illustrated in Fig. 4.

For the ith arm:

$$\begin{aligned} T_{i1} &= (F_{fi1} - F_{ei1})r + (F_{fi3} - F_{ei3})r \\ T_{i2} &= (F_{fi2} - F_{ei2})r + (F_{fi3} - F_{ei3})r \\ &\quad +(F_{fi4} - F_{ei4})r + (F_{fi5} - F_{ei5})r \\ T_{i3} &= (F_{fi5} - F_{ei5})r + (F_{fi6} - F_{ei6}) \end{aligned} \tag{13}$$

In Eq. (13), r represents the joint radius. The forces F_{fij} and F_{eij} correspond to the outputs of the flexor and extensor muscles, respectively, and can be calculated as given in Eq. (14):

$$\begin{aligned} F_{fij} &= u_{fij} - ku_{fij}x - bu_{fij}\dot{x} \\ F_{eij} &= u_{eij} + ku_{eij}x + bu_{eij}\dot{x} \end{aligned} \quad (14)$$

where u_{fi}, u_{ei} are contractile forces or activation levels generated by flexor and extensor muscles, for i = 1–3. Note that joint angle q may create two different contacting lengths x due to the different direction in two muscles: $x = -rq$ for the flexor muscle and $x = rq$ for the extensor muscle. By substituting Eq. (14) into Eq. (13), the joint torques are obtained as shown in Eq. (15):

$$\begin{aligned} T_{i1} &= (u_{fi1} - u_{ei1})r - (u_{fi1} + u_{ei1})kr^2q_{i1} \\ &-(u_{fi1} + u_{ei1})br^2\dot{q}_{i1} + (u_{fi3} - u_{ei3})r \\ &-(u_{fi3} + u_{ei3})kr^2(q_{i1} + q_{1i}) \\ &-(u_{fi3} + u_{ei3})br^2(\dot{q}_{i1} + \dot{q}_{i2}) \\ T_{i2} &= (u_{fi2} - u_{ei2})r - (u_{fi2} + u_{ei2})kr^2q_{i2} \\ &-(u_{fi2} + u_{ei2})br^2\dot{q}_{i2} + (u_{fi3} - u_{ei3})r \\ &-(u_{fi3} + u_{ei3})kr^2(q_{i1} + q_{i2}) \\ &-(u_{fi3} + u_{ei3})br^2(\dot{q}_{i1} + \dot{q}_{i2}) \\ &+(u_{fi4} - u_{ei4})r - (u_{fi4} + u_{ei4})kr^2q_{i2} \\ &-(u_{fi4} + u_{ei4})br^2\dot{q}_{i2} + (u_{fi5} - u_{ei5})r \\ &-(u_{fi5} + u_{ei5})kr^2(q_{i2} + q_{i3}) \\ &-(u_{fi5} + u_{ei5})br^2(\dot{q}_{i2} + \dot{q}_{i3}) \\ T_{i3} &= (u_{fi5} - u_{ei5})r - (u_{fi5} + u_{ei5})kr^2(q_{i2} + q_{i3}) \\ &-(u_{fi5} + u_{ei5})br^2(\dot{q}_{i2} + \dot{q}_{i3}) + (u_{fi6} - u_{ei6})r \\ &-(u_{fi6} + u_{ei6})kr^2q_{i3} - (u_{fi6} + u_{ei6})br^2\dot{q}_{i3} \end{aligned} \quad (15)$$

The antagonistic mono-articular muscles maintained near-maximal activation throughout changes in the direction of the output force. In contrast, the bi-articular muscle pair exhibited a criss-cross activation pattern. The muscle activation levels required to generate the maximum output force at the end-effector E are defined as given in Eq. (16) [23]:

$$u_{fij} + u_{eij} = 100\%\ for\ i = 1-2, j = 1-6 \quad (16)$$

Since the contractile force of the flexor muscle u_{fi} can be actively controlled by an actuator, the resulting muscle torques are expressed in Eqs. (17) and (18) [12]:

$$\begin{aligned} T_i &= \begin{bmatrix} T_{i1} \\ T_{i2} \\ T_{i3} \end{bmatrix} = \begin{bmatrix} \tau_{i1} \\ \tau_{i2} \\ \tau_{i3} \end{bmatrix} \\ &-r^2\begin{bmatrix} k_1 + k_3 & k_3 & 0 \\ k_3 & k_2 + k_3 + k_4 + k_5 & k_5 \\ 0 & k_5 & k_4 + k_5 \end{bmatrix} q_i \\ &-r^2\begin{bmatrix} b_1 + b_3 & b_3 & 0 \\ b_3 & b_2 + b_3 + b_4 + b_5 & b_5 \\ 0 & b_5 & b_5 + b_6 \end{bmatrix} \dot{q}_i \end{aligned} \quad (17)$$

where:

$$\begin{aligned} \tau_i &= \begin{bmatrix} \tau_{i1} \\ \tau_{i2} \\ \tau_{i3} \end{bmatrix} \\ &= r\begin{bmatrix} 2(u_{fi1} - 1) + 2(u_{fi3} - 1) \\ 2(u_{fi2} - 1) + 2(u_{fi3} - 1) + 2(u_{fi4} - 1) + 2(u_{fi5} - 1) \\ 2(u_{fi5} - 1) + 2(u_{fi6} - 1) \end{bmatrix} \end{aligned} \quad (18)$$

Then, Eq. (17) can be expressed in the form of Eq. (19).

$$T = \begin{bmatrix} T_1 \\ T_2 \end{bmatrix} = \begin{bmatrix} \tau_{1i} \\ \tau_{2i} \end{bmatrix} - r^2\begin{bmatrix} K_1 & 0 \\ 0 & K_2 \end{bmatrix} q - r^2\begin{bmatrix} B_1 & 0 \\ 0 & B_2 \end{bmatrix} \dot{q} \quad (19)$$

where K_i and B_i are defined in Eqs. (20) and (21), respectively.

$$K_i = \begin{bmatrix} k_1 + k_3 & k_3 & 0 \\ k_3 & k_2 + k_3 + k_4 + k_5 & k_5 \\ 0 & k_5 & k_4 + k_5 \end{bmatrix} \quad (20)$$

$$B_i = \begin{bmatrix} b_1 + b_3 & b_3 & 0 \\ b_3 & b_2 + b_3 + b_4 + b_5 & b_5 \\ 0 & b_5 & b_4 + b_5 \end{bmatrix} \quad (21)$$

It is evident that both K_i and B_i are positive definite matrices. By substituting Eq. (19) into Eq. (10), the dynamic equation of the dual-arm system can be expressed as Eq. (22):

$$\begin{aligned} \tau_i &= H_i(q_i)\ddot{q}_i + \left(\frac{1}{2}\dot{H}(q_i) + S(q_i, \dot{q}_i)\right)\dot{q}_i \\ &+J_{0i}^T\begin{pmatrix} cos(\theta + \theta_i) \\ sin(\theta + \theta_i) \end{pmatrix} f_i \\ &+\left(re_i - J_{0i}^T\begin{pmatrix} sin(\theta + \theta_i) \\ -cos(\theta + \theta_i) \end{pmatrix}\right)\lambda_i + r^2K_iq_i + r^2B_i\dot{q}_i \end{aligned} \quad (22)$$

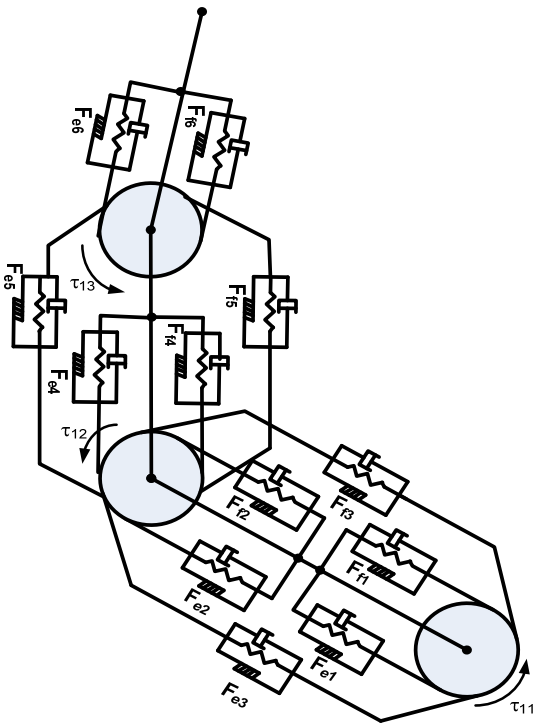

Fig. 4. Phenomenological model of ith arm.

This allows the formulation of the control problem, which consists of two main objectives:

(1) Maintaining a stable grasp on the object;
(2) Rotating it to the desired orientation and positioning it at the target location.

D. Control Law for Stable Grasping

Stable grasping can be achieved when sum of forces and moments apply on the object equal to zero and the normal contact forces for securely keeping the object attained the desired contact force. The first control inputs u_{fi} (for i = 1, 2) for maintaining the desired contact force f_d are given in Eq. (23):

$$u_{fi} = J_{0i}^T \begin{bmatrix} cos\,\theta \\ -sin\,\theta \end{bmatrix} f_d + r f_d \sin\theta_i\, e_3 - K_{vi}\dot{q}_i + K_i q_i \quad (23)$$

Then control u_{mi} (i = 1, 2) is for balancing the moments applying on the object and is proposed as given in Eq. (24).

$$u_{mi} = (-1)^i \frac{cos\,\theta_i}{\sum_{i=1}^{2}(-1)^i cos\,\theta_i} f_d R(sin\,\theta_1 - sin\,\theta_2)e_3 \quad (24)$$

Applying principle of superposition, a control input for stable grasping $u_i = u_{fi} + u_{mi}$ is proposed and substituted into the dynamic Eq. (10) of the dual-arm system, the closed-loop dynamics of the system can be expressed as Eq. (25):

$$\begin{aligned} &\left(H_i(q_i)\frac{d}{dt} + \frac{1}{2}\dot{H}_i(q_i) + S_i(q_i,\dot{q}_i) + (Kv_i + B_i)\right)\dot{q}_i \\ &\quad = -J_{oi}^T \begin{bmatrix} cos(\theta+\theta_i) \\ -sin(\theta+\theta_i) \end{bmatrix} \Delta f_i \\ &\quad + \left(J_{0i}^T \begin{bmatrix} sin(\theta+\theta_i) \\ cos(\theta+\theta_i) \end{bmatrix} - re_3\right)\Delta\lambda_i \\ &\quad -(1)^i \frac{cos\,\theta_i}{\sum_{i=1}^{2} cos\,\theta_i} f_d R(sin\,\theta_1 - sin\,\theta_2)e_3 \end{aligned} \quad (25)$$

where contact force errors Δf_i are defined as:

$$\begin{aligned} \Delta f_i &= f_i - f_d\, cos(\theta_i + \theta) \\ \Delta\lambda_i &= f_i - f_d\, sin(\theta_i + \theta) \end{aligned} \quad (26)$$

Substituting Eq. (26) into Eq. (11) yields Eq. (27):

$$\begin{aligned} &M\ddot{x} + \sum_{i=1}^{2}\Delta f_i\, cos(\theta+\theta_i) + \sum_{i=1}^{2}\Delta\lambda_i\, sin(\theta_i+\theta) = 0 \\ &M\ddot{y} + \sum_{i=1}^{2}\Delta f_i\, cos(\theta+\theta_i) - \sum_{i=1}^{2}\Delta\lambda_i\, sin(\theta_i+\theta) = 0 \\ &I\ddot{\theta} - (\Delta\lambda_1 - \Delta\lambda_2)R - f_d(Y_1 - Y_2) = 0 \end{aligned} \quad (27)$$

where Y_i is determined by Eq. (28):

$$Y_i = R\, sin(\theta + \theta_i) \quad (28)$$

Differentiating Eq. (3) to leads to Eq. (29):

$$\dot{\theta}_i = \frac{r}{r+R}\dot{q}_i^T e_3 - \frac{r}{R+r}\dot{\theta} \quad (29)$$

Differentiating Eq. (28) and substituting Eq. (29) into the resulting equation yields Eq. (30):

$$\frac{\dot{Y}_1 - \dot{Y}_2}{k_1 - k_2} = \frac{k_1}{k_1 - k_2}\dot{q}_1^T e_3 - \frac{k_2}{k_1 - k_2}\dot{q}_2^T e_3 - \dot{\theta} \quad (30)$$

where k_i is determined by Eq. (31):

$$k_i = \frac{Rr\,cos(\theta+\theta_i)}{r+R} \quad (31)$$

Since the left arm workspace is confined in the left side of the circular object and the right arm is confined in the right side, this leads to Eq. (32):

$$\begin{aligned} \pi/2 < \theta + \theta_1 < 3\pi/2 \\ -\pi/2 < \theta + \theta_2 < \pi/2 \end{aligned} \quad (32)$$

and the term (k_1−k_2) is always positive.

By implementing in the following way:

$$\sum_{i=1}^{2} \dot{q}_i^T \times Eq.(25) + \left[\dot{x}, \dot{y}, \dot{\theta}\right] \times Eq.(27)$$

and referring to Eq. (22), Eq. (33) can be obtained:

$$\begin{aligned} &\dot{q}_1^T \times (-\tau_{m1}) + \dot{q}_2^T \times (-\tau_{m2}) \\ &\quad = \frac{f_d}{2(k_1 - k_2)}\frac{d}{dt}(Y_1 - Y_2)^2 \end{aligned} \quad (33)$$

Differentiating constraints Q_i (Eq. (6)) and R_i (Eq. (7)) yields Eqs. (34) and (35):

$$\sum_{i=1}^{2} f_i \left(\dot{q}_i^T \frac{\partial Q_i}{\partial q_i} + \dot{x}\frac{\partial Q_i}{\partial x} + \dot{y}\frac{\partial Q_i}{\partial y} + \dot{\theta}\frac{\partial Q_i}{\partial \theta}\right) = 0 \quad (34)$$

$$\sum_{i=1}^{2} \lambda_i \left(\dot{q}_i^T \frac{\partial R_i}{\partial q_i} + \dot{x}\frac{\partial R_i}{\partial x} + \dot{y}\frac{\partial R_i}{\partial y} + \dot{\theta}\frac{\partial R_i}{\partial \theta}\right) = 0 \quad (35)$$

By taking the inner products $\dot{q}_i$ with Eq. (25) and $\dot{q}_i, \dot{z} = (\dot{x}, \dot{y}, \dot{\theta})^T$ with Eq. (27), respectively, and summing the resulting expressions, while referencing Eqs. (8), (9), (33), (34), and (35), the following relationship can be derived as Eq. (36):

$$\frac{d}{dt}E_1 = -\sum_{i=1}^{2} \dot{q}_i{}^T (K_{vi} + B_i)\,\dot{q}_i \quad (36)$$

where E_1 is determined by Eq. (37):

$$E_1 = \frac{1}{2}\begin{pmatrix} \sum_{i=1}^{2} \dot{q}_i^T H_i(q_i)\dot{q}_i + M\dot{x}^2 \\ +M\dot{y}^2 + I\dot{\theta}^2 + \frac{f_d(Y_1 - Y_2)^2}{(k_1 - k_2)} \end{pmatrix} \quad (37)$$

It is clear that E_1 is non-negative function in $\dot{q}_i, \dot{z} = (\dot{x}, \dot{y}, \dot{\theta})^T$ and $(Y_1 - Y_2)$. Since $\dot{z}, \dot{q}_i$ are norm-bounded in $L^2(0, \infty)$, position vectors q and z must be bounded and then $\ddot{z}, \ddot{q}_i$ uniform bounded. By choosing control damping matrix K_{vi} such that matrix (K_{vi}+B_i) is positive definite function, Eq. (36) guarantees that E_1 will be non-increasing function and implies that $\dot{q}_i \to 0$ as $t \to \infty$, then the right-hand side of Eq. (25) comes to

zero. Then the vector $J_{0i}^T[cos(\theta+\theta_i), sin(\theta+\theta_i)^T, J_{0i}^T[sin(\theta+\theta_i), cos(\theta+\theta_i)^T$ and $cos(\theta+\theta_i)/\sum_{i=1}^{2} cos(\theta+\theta_i)$ are independent. Then Eq. (25) equals zero only when:

$$\begin{cases} \Delta f_i = f_i - f_d\, cos(\theta+\theta_i) \to 0 \\ \Delta \lambda_i = \lambda_i - f_d\, sin(\theta+\theta_i) \to 0 \\ f_d(Y_1 - Y_2) \to 0 \end{cases}$$

This result confirms that both force and moment balance are achieved, which guarantees stable grasping of the object and prevents further sliding or rotation under the proposed control input. Based on this, a control algorithm is formulated to regulate the position of the grasped object, ensuring that its center of mass reaches the desired coordinates x_d and y_d along the x-axis and y-axis of the {oxy} coordinate frame.

E. Control Law for Desired Position of the Grasping Object

From Fig. 2, the geometrical relations can be derived and expressed as Eqs. (38) and (39):

$$\begin{cases} x = x_{01} + (R+r)\, cos(\theta+\theta_1) \\ \quad = x_{02} + (R+r)\, cos(\theta+\theta_2) \end{cases} \tag{38}$$

$$\begin{cases} y = y_{01} + (R+r)\, sin(\theta+\theta_1) \\ \quad = y_{02} - (R+r)\, sin(\theta+\theta_2) \end{cases} \tag{39}$$

By differentiating Eq. (38) and performing the necessary transformations, the following result is obtained:

$$\begin{gathered} \dot{x} = \dot{q}_1^T \left(J_{01}^T \begin{bmatrix} 1 \\ 0 \end{bmatrix} - r\, sin(\theta+\theta_1) e_3 \right) \\ \frac{sin(\theta+\theta_2)}{sin(\theta+\theta_2) - sin(\theta+\theta_1)} \\ + \dot{q}_2^T \left(J_{02}^T \begin{bmatrix} 0 \\ 1 \end{bmatrix} + r\, sin(\theta+\theta_2) e_3 \right) \\ \frac{sin(\theta+\theta_1)}{sin(\theta+\theta_2) - sin(\theta+\theta_1)} \end{gathered} \tag{40}$$

Based on Eq. (40), a control law u_{xi} is proposed to regulate the object's center of mass toward the desired coordinate x_d, defined in Eq. (41):

$$\begin{cases} u_{x1} = \left(J_{01}^T \begin{bmatrix} 1 \\ 0 \end{bmatrix} - r\, sin(\theta+\theta_1) e_3 \right) \frac{K_x (x - x_d)\, sin(\theta+\theta_2)}{sin(\theta+\theta_2) - sin(\theta+\theta_1)} \\ u_{x2} = \left(J_{02}^T \begin{bmatrix} 1 \\ 0 \end{bmatrix} - r\, sin(\theta+\theta_2) e_3 \right) \frac{K_x (x - x_d)\, sin(\theta+\theta_1)}{sin(\theta+\theta_2) - sin(\theta+\theta_1)} \end{cases} \tag{41}$$

From Eq. (41), Eq. (42) can be obtained as follows:

$$-\sum_{i=1}^{2} \dot{q}_i^T\, u_{xi} = K_x \frac{(x - x_d)^2}{2} \tag{42}$$

Similar transformation with Eq. (39) can be resulting:

$$\begin{gathered} \dot{y} = \dot{q}_1^T \left(J_{01}^T \begin{bmatrix} 1 \\ 0 \end{bmatrix} - r\, cos(\theta+\theta_1) e_3 \right) \\ \frac{cos(\theta+\theta_2)}{cos(\theta+\theta_2) + cos(\theta+\theta_1)} \\ + \dot{q}_2^T \left(J_{02}^T \begin{bmatrix} 0 \\ 1 \end{bmatrix} + r\, cos(\theta+\theta_2) e_3 \right) \\ \frac{cos(\theta+\theta_1)}{cos(\theta+\theta_2) + cos(\theta+\theta_1)} \end{gathered} \tag{43}$$

Based on Eq. (43), a control law u_{yi} is proposed to regulate the object's center of mass toward the desired coordinate y_d, expressed in Eq. (44):

$$\begin{cases} u_{y1} = \left(J_{01}^T \begin{bmatrix} 1 \\ 0 \end{bmatrix} - r\, cos(\theta+\theta_1) e_3 \right) \frac{K_y (y - y_d)\, cos(\theta+\theta_2)}{cos(\theta+\theta_2) + cos(\theta+\theta_1)} \\ u_{y2} = \left(J_{01}^T \begin{bmatrix} 1 \\ 0 \end{bmatrix} - r\, cos(\theta+\theta_1) e_3 \right) \frac{K_y (y - y_d)\, cos(\theta+\theta_1)}{cos(\theta+\theta_2) + cos(\theta+\theta_1)} \end{cases} \tag{44}$$

where K_x, K_y is a diagonal positive matrix.

It is possible to have:

$$-\sum_{i=1}^{2} \dot{q}_i^T\, u_{yi} = K_y \frac{(y - y_d)^2}{2}$$

Building upon the premise that complex dexterous movements can be decomposed into a set of fundamental motion primitives that can be independently acquired and executed, the overall control input for a complete motion is synthesized through the principle of linear superposition. Specifically, the control input is formulated as a combination of the components u_{fi}, u_{xi}, and u_{yi}, as described in Eq. (45):

$$u_i = u_{fi} + u_{mi} + u_{xi} + u_{yi} \tag{45}$$

By substituting u_i from Eq. (44) into the dynamic equations of the overall system and performing the necessary transformations, the following relation is obtained as Eq. (46):

$$\frac{d}{dt} E_2 = -\sum_{i=1}^{2} \dot{q}_i^T K_{vi} \dot{q}_i - \alpha \dot{\theta}^2 \tag{46}$$

where $E_2 = E_1 + \frac{K_y (y - y_d)^2}{2} + \frac{K_x (x - x_d)^2}{2}$.

It is clear that function E_2 is non-negative function in $\dot{q}_i, \dot{z} = (\dot{x}, \dot{y}, \dot{\theta})^T$, $(Y_1 - Y_2)$ and $(y - y_d)$ and $(x - x_d)$. According to Lyapunov stability theorem, the convergence of the system can be demonstrated as shown in Eq. (47):

$$\begin{cases} \dot{q}_1, \dot{q}_2, \dot{x}, \dot{y}, \dot{\theta} \to 0 \\ \Delta f_1 = f_1 - f_{d1} = f_1 - f_d\, cos(\theta+\theta_1) \to 0 \\ \Delta f_2 = f_2 - f_{d2} = f_2 - f_d\, cos(\theta+\theta_2) \to 0 \\ \Delta \lambda_1 = \lambda_1 - \lambda_{d1} = \lambda_1 - f_d\, sin(\theta+\theta_1) \to 0 \\ \Delta \lambda_2 = \lambda_2 - \lambda_{d2} = \lambda_2 - f_d\, sin(\theta+\theta_2) \to 0 \\ Y_1 - Y_2 \to 0 \\ \Delta x = x - x_d \to 0 \\ \Delta y = y - y_d \to 0 \end{cases} \tag{47}$$

as $t \to \infty$.

That means the objective of propose control for stable grasping and dexterous manipulating the object has been achieved.

IV. Simulation Results

In this simulation, the dual-finger robot is tasked with manipulating a circular object on a horizontal plane. The robot must securely grasp the object and transport it to a designated position within the workspace. Initially, the joint positions of both the dual-finger robot and the object are configured to satisfy the grasping constraints and maintain a stable grasp. The parameters of the dual-finger robot and the manipulated object are listed in Table I. The mass and length of the arms are chosen to approximate those of an average human multi-fingered hand, thereby enhancing the anthropomorphic fidelity of the simulation.

TABLE I. Physical Parameters

Notation	Sym	Value	Unit
Mass of 1st link	m_{i1}	0.0385	[kg]
Mass of 2nd link	m_{i2}	0.032	[kg]
Mass of 3rd link	m_{i3}	0.026	[kg]
Length of 1st link	l_{i1}	0.077	[m]
Length of 2nd link	l_{i2}	0.064	[m]
Length of 3rd link	l_{i3}	0.052	[m]
Mass of the object	M	0.05	[kg]
Radius of object	R	0.037	[m]
Elastic coefficient	k	3000	[N/m]
Viscous coefficient	b	400	[Ns/m]
Radius of joint i	r	0.02	[m]

The Constraint Stabilization Method (CSM) is employed to capture the system's dynamic behavior accurately. CSM is a numerical technique commonly used in the simulation of mechanical systems subject to kinematic or dynamic constraints. In such systems, constraint equations may be violated due to numerical inaccuracies or the accumulation of integration errors over time, leading to constraint drift and potentially unstable or unreliable simulation outcomes. To address these issues, CSM introduces auxiliary conditions into the system's equations of motion and applies correction terms to reduce constraint deviations. Among the various stabilization strategies, the Baumgarte Stabilization Method is widely adopted [26]. This approach modifies the constraint equations by incorporating damping and stiffness-like terms, as shown in Eq. (48):

$$\begin{aligned} \ddot{R}_1 + \gamma_1 \dot{R}_1 + \omega_1 R_1 = 0 \\ \ddot{R}_2 + \gamma_1 \dot{R}_2 + \omega_1 R_2 = 0 \end{aligned} \tag{48}$$

where γ_i, ω_i are tuning parameters selected to achieve the desired level of stability. The underlying concept is to reformulate the constraint dynamics as a damped oscillatory system, thereby enabling the system to naturally converge toward a constraint-satisfying state over time. Then Eq. (48) is integrated into the closed-loop dynamic system to perform simulations and evaluate the system's characteristics when the proposed control algorithm is applied.

The control parameters used in the simulation are presented in Table II.

TABLE II. Control Parameters

Symbol	Notation	Value
K_{vi} (i = 1, 2)	D-gain	0.075
γ_{λ_i}	Constraint Stabilization Method (CSM) parameter	160
$\omega_{\lambda i}$	CSM parameter	80
Γ_x	P-gain	0.15
Γ_y	P-gain	0.15
f_d	desired force	1 N
x_d	Desired position in x-axis	0.099 m
y_d	Desired position in y-axis	0.085 m

To validate the effectiveness of the proposed control laws, numerical simulations were conducted using MATLAB. The analysis focuses on the behavior of key physical quantities, including the normal contact forces f_1 and f_2 acting on the object surfaces, the moment applied to the object $f_d(Y_1\text{-}Y_2)$, the rotational velocity, and the translational velocities of the object.

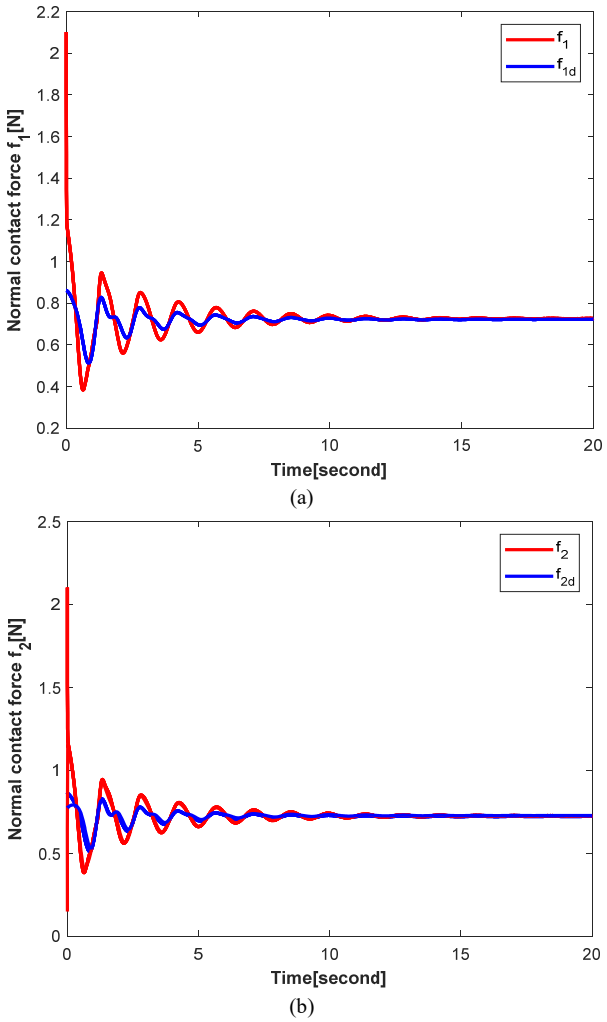

Fig. 5. Normal contact force f_1 (a) and f_2 (b).

Fig. 5 illustrates the time responses of the normal contact forces f_1 and f_2, respectively. The results show that

both forces converge to their desired values f_{1d}, f_{2d} within approximately 10 s, confirming the effectiveness of the force control scheme. Similarly, the tangential contact forces λ_1 and λ_2 closely follow their corresponding reference values λ_{1d} and λ_{2d}, as depicted in Fig. 6. The results in Fig. 7 show that both the rotational and translational velocities converge to zero, indicating that the object ceases rotation and translation around the 10 s. This result demonstrates that the object becomes fully stationary under the influence of the proposed control law. Correspondingly, the moment applied to the grasped object, illustrated in Fig. 8, also stabilizes at zero, confirming the complete cessation of motion. These findings confirm that stable grasping of the object has been successfully achieved using the dual-finger PAM-driven robot.

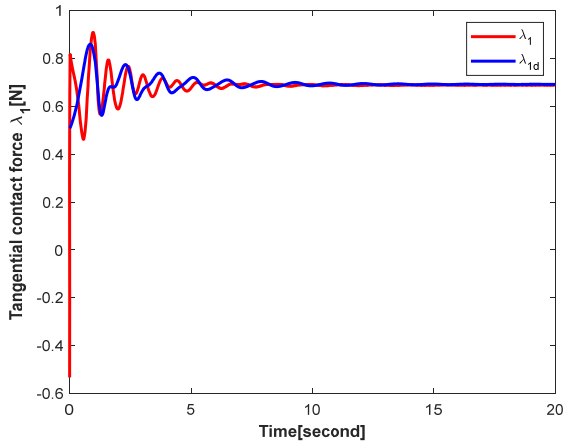

(a)

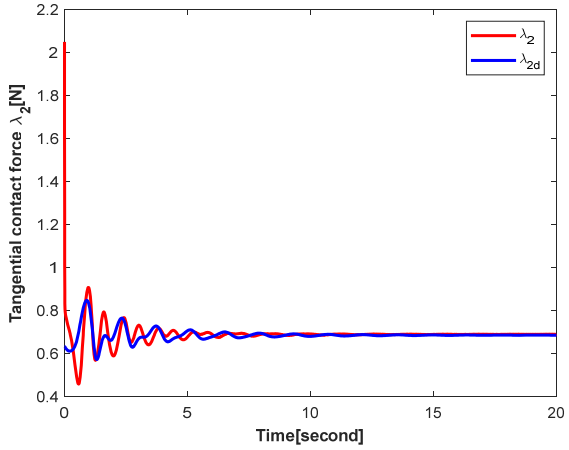

(b)

Fig. 6. Tangential contact force λ_1 (a) and λ_2 (b).

Additionally, Fig. 9 illustrates the asymptotic convergence of the object's actual position to its desired reference trajectory across both x- and y-axis coordinates. This effective positional tracking, alongside the previously demonstrated regulation of force and velocity, validates the dual capabilities of the control algorithm. Specifically, it ensures stable grasp conditions through appropriate force distribution while also achieving precise positional control within the task space. These simulation results generally confirm that the proposed control strategy facilitates robust grasping and accurate manipulation of the target object. However, the effectiveness of the algorithm remains limited to theoretical validation, due to several reasons: to simplify the validation of the proposed control algorithms on the robot-object dynamic system, this study assumes ideal conditions by neglecting the effects of disturbances, uncertainties in kinematic and dynamic parameters, and actuator delays. Theoretically, the proposed control algorithms have not yet demonstrated asymptotic stability of the closed-loop dynamic system under the influence of external disturbances and system uncertainties.

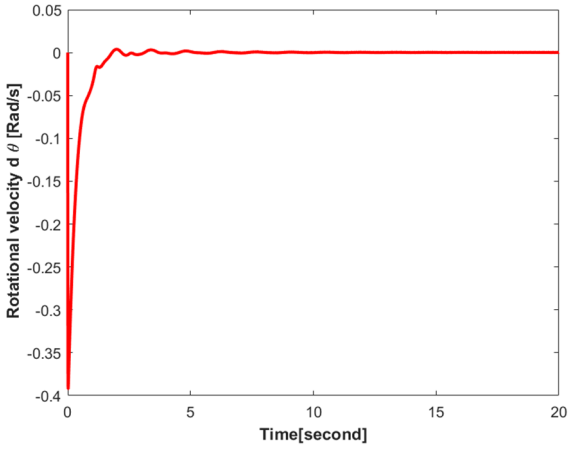

(a)

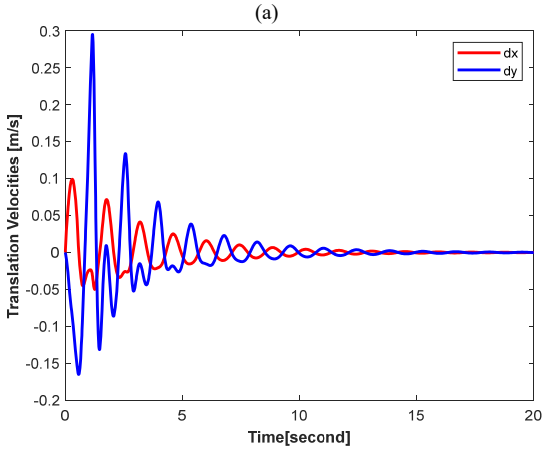

(b)

Fig. 7. Rotational velocity (a) and translational velocities (b) of the grasped object.

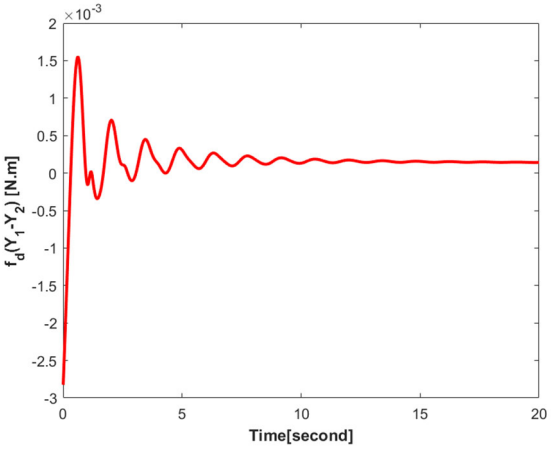

Fig. 8. Applied moment on the object.

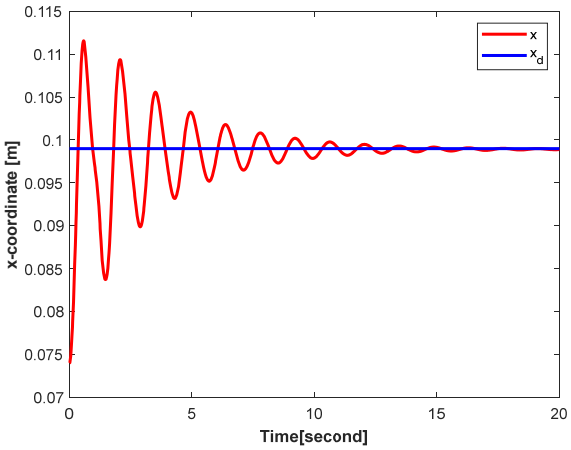

(a)

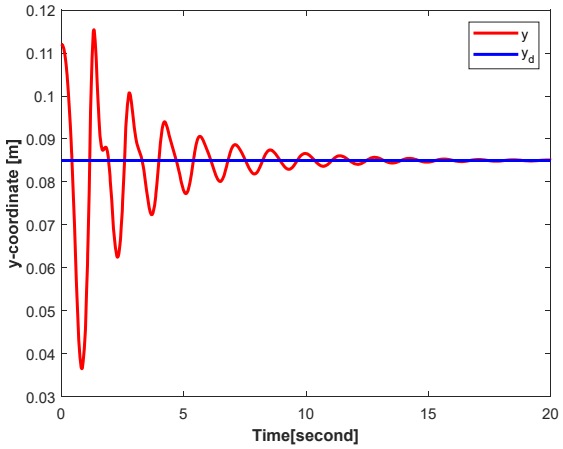

(b)

Fig. 9. Coordinate of center-mass of the object in (a) x-axis and (b) y-axis.

Developing a multi-fingered robotic system driven by PAMs involves several complex challenges. Primary factors, such as pneumatic delays, nonlinear friction, sensor noise, and parameter mismatches, must be considered and evaluated via simulation. Then the system requires precise hardware integration, stable air pressure regulation, and real-time data acquisition systems capable of handling multiple degrees of freedom. Ensuring mechanical robustness while maintaining modularity for testing different configurations is also critical. These challenges must be addressed to validate control strategies under realistic operating conditions and to bridge the gap between simulation and practical deployment.

It is confirmed from simulation works that the proposed control algorithms facilitate stable grasping during robot–object interaction by ensuring that the contact forces are consistently maintained at the required states. These states are derived from the static stability condition of the grasped object, where the resultant forces and moments acting on the object's center of mass are zero. The controller is designed based on the principle of linear superposition of input signals and its stability has been rigorously proven using Lyapunov and LaSalle stability criteria. Simulation results have further demonstrated that the robot achieves both stable grasp and dexterous object manipulation. This capability represents a critical step toward transitioning from simulation to an experimental robotic system designed for motor function rehabilitation in elderly individuals or patients. By automatically regulating the contact forces between the robotic fingers and the object, the system can ensure user safety while enabling appropriate and effective training exercises.

V. Conclusions

This study develops a control framework for a dual-arm robot actuated by Pneumatic Artificial Muscles (PAMs) to grasp and manipulate circular objects stably. Using the Lagrange method and Hamilton's principle, the derived control laws ensure asymptotic stability of object motion and contact forces, as proven via Lyapunov theory and LaSalle's invariance principle.

The effectiveness of the proposed control strategy is verified through detailed numerical simulations in MATLAB. Results show that the normal and tangential contact forces converge rapidly to their desired values, while both rotational and translational velocities of the object diminish to zero within six seconds, indicating a fully stabilized grasp. The applied moment on the object also converges to zero, and the object's center of mass asymptotically tracks the desired trajectory along both spatial axes. These outcomes collectively demonstrate the controller's ability to simultaneously ensure grasp stability and precise object positioning.

The novelty of this research lies in developing control algorithms for stable grasping and dexterous manipulation of grasped objects using a dual-finger PAM-driven robotic system. Unlike conventional approaches that rely on force sensors to regulate contact forces, the proposed method achieves desired contact force control without force sensing, inspired by human blind grasping behavior. This sensor-less force regulation is possible through a model-based control strategy that leverages kinematic transformations and Lyapunov-based stability analysis.

Furthermore, the system is designed to operate under idealized conditions—on a horizontal plane and without gravitational influence—allowing simplification of the dynamic model and reducing dependency on uncertain parameters. Simulation results demonstrate the algorithm's robustness to small disturbances, and future work will extend the framework to incorporate adaptive and robust control mechanisms for more complex interaction scenarios.

In future work, the proposed framework could be extended to accommodate more complex object geometries, uncertainties in model parameters, and real-time implementation on physical robot platforms. In addition, future studies may involve the development of experimental systems to validate the theoretical findings.

Conflict of Interest

The authors declare no conflict of interest.

Author Contributions

SH conducted the research, developed the dynamic model, and performed the control design; PTAN

supervised the study and provided critical revisions; CCT performed the simulations, analyzed the results, and contributed to manuscript preparation; all authors had approved the final version.

ACKNOWLEDGEMENT

The author sincerely appreciates the invaluable support provided by the Faculty of Electronics Engineering 1 and the Automation and Robotics Laboratory at the Posts and Telecommunications Institute of Technology (PTIT), Hanoi, Vietnam, in the completion of this study.

REFERENCES

[1] A. Hentout, M. Aouache, A. Maoudj *et al.,* "Human–robot interaction in industrial collaborative robotics: A literature review of the decade 2008–2017," *Advanced Robotics*, vol. 33, no. 15–16, pp. 764–799, 2019.

[2] B. Butsanlee, W. Pongaen, N. Rothong *et al.,* "Development of deep learning for power energy optimization in the industrial robot system," *International Journal of Mechanical Engineering and Robotics Research*, vol. 13, no. 2, pp. 254–265, 2024.

[3] D. Rodriguez-Guerra, G. Sorrosal, I. Cabanes *et al.,* "Human-robot interaction review: Challenges and solutions for modern industrial environments," *IEEE Access*, vol. 9, pp. 108557–108578, 2021.

[4] Z. Ye, L. Zheng, W. Chen *et al.,* "Recent advances in bioinspired soft robots: fabrication, actuation, tracking, and applications," *Advanced Materials Technologies*, vol. 9, no. 21, 2301862, 2024.

[5] B. Kalita, A. Leonessa, and S. K. Dwivedy, "A review on the development of pneumatic artificial muscle actuators: Force model and application," *Actuators*, vol. 11, no. 10, 288, 2022.

[6] G. K. Klute, J. M. Czerniecki, and B. Hannaford. "Artificial muscles: Actuators for biorobotic systems," *The International Journal of Robotics Research*, vol. 21, no. 4, pp. 295–309, 2002.

[7] D. G. Caldwell, G. A. Medrano-Cerda, and M. Goodwin. "Control of pneumatic muscle actuators," *IEEE Control Systems Magazine*, vol. 15, no. 1, pp. 40–48, 1995.

[8] P. B. Banyarani, B. Tarvirdizadeh, and A. Hadi. "Design and fabrication of a soft wearable robot using a novel pleated fabric Pneumatic Artificial Muscle (pfPAM) to assist walking," *Sensors and Actuators A: Physical*, vol. 370, 115278, 2024.

[9] B. Jamil, N. Oh, J.-G. Lee *et al.,* "A review and comparison of linear pneumatic artificial muscles," *International Journal of Precision Engineering and Manufacturing-Green Technology*, vol. 11, no. 1, pp. 277–289, 2024.

[10] C. V. Baysal, "Implementation of rehabilitation modalities using a low-cost PAM actuated robotic orthosis," *IEEE Access*, vol. 11, pp. 103601–103615, 2023.

[11] D. Reynolds, D. Repperger, C. Phillips *et al.,* "Modeling the dynamic characteristics of pneumatic muscle," *Annals of Biomedical Engineering*, vol. 31, no. 3, pp. 310–317, 2003.

[12] M. Kumamoto, T. Oshima, and T. Yamamoto. "Control properties induced by the existence of antagonistic pairs of bi-articular muscles—Mechanical engineering model analyses," *Human Movement Science*, vol. 13, no. 5, pp. 611–634, 1994.

[13] S. Oh and Y. Hori, "Development of two-degree-of-freedom control for robot manipulator with biarticular muscle torque," in *Proc. 2009 American Control Conf.*, 2009, pp. 325–330.

[14] H. Kawai, T. Murao, R. Sato *et al.,* "Passivity-based control for 2DOF robot manipulators with antagonistic bi-articular muscles," in *Proc. 2011 IEEE International Conf. on Control Applications (CCA)*, 2011, pp. 1451–1456.

[15] Y. Kawai, H. Kawai, and M. Fujita, "RISE control for 2DOF human lower limb with antagonistic bi-articular muscles," in *Proc. 2013 IEEE International Conf. on Control Applications (CCA),* 2013, pp. 109–114.

[16] Y. Wang, W. Wang, and G. Bao, "Design and control scheme of a rigid-flexible coupled Duel-Arm hug robots," in *Proc. 2024 IEEE-RAS 23rd International Conf. on Humanoid Robots (Humanoids)*, 2024, pp. 1027–1033.

[17] Y. Wang and Q. Xu, "Design and fabrication of a new dual-arm soft robotic manipulator," *Actuators*, vol. 8, no. 1, 5, 2019.

[18] H. Li, D. Gong, and J. Yu, "Control of robotic joint actuated by antagonistic pneumatic artificial muscles based on model-free reinforcement learning," in *Proc. 2021 IEEE International Conf. on Robotics and Biomimetics (ROBIO)*, 2021, pp. 887–892.

[19] V. E. Abarca and D. A. Elias, "A review of parallel robots: Rehabilitation, assistance, and humanoid applications for neck, shoulder, wrist, hip, and ankle joints," *Robotics*, vol. 12, no. 5, 131, 2023.

[20] P. Zhang, W. Chen, and B. Tang, "Design and feasibility tests of a lightweight soft gripper for compliant and flexible envelope grasping," *Soft Robotics*, vol. 9, no. 2, pp. 376–385, 2022.

[21] N. Ahmad, M. Usama, H. Iqbal *et al.,* "Design and development of a three fingered under actuated prosthetic hand," in *Proc. 2024 International Conf. on Robotics and Automation in Industry (ICRAI)*, 2024, pp. 1–6.

[22] C. Yu and P. Wang, "Dexterous manipulation for multi-fingered robotic hands with reinforcement learning: A review," *Frontiers in Neurorobotics*, vol. 16, 861825, 2022.

[23] C.-P. Chou and B. Hannaford, "Measurement and modeling of McKibben pneumatic artificial muscles," *IEEE Transactions on Robotics and Automation*, vol. 12, no. 1, pp. 90–102, 1996.

[24] Z. Zhou, Q. Ai, M. Li *et al.,* "The design and adaptive control of a parallel chambered pneumatic muscle-driven soft hand robot for grasping rehabilitation," *Biomimetics*, vol. 9, no. 11, 706, 2024.

[25] H. P. H. Anh, C. Van Kien, and N. T. Nam, "Advanced force control of the 2-axes PAM-based manipulator using adaptive neural networks," *Robotica*, vol. 36, no. 9, pp. 1333–1362, 2018.

[26] J. Baumgarte, "Stabilization of constraints and integrals of motion in dynamical systems," *Computer Methods in Applied Mechanics and Engineering*, vol. 1, no. 1, pp. 1–16, 1972.